Journal of CO2 Utilization 79 (2024) 102653

Contents lists available at ScienceDirect

Journal of CO2 Utilization

journal homepage: www.elsevier.com/locate/jcou

Synthetic natural gas production using CO_2-rich waste stream from hydrothermal carbonization of biomass: Effect of impurities on the catalytic activity

J. González-Arias [a,*], G. Torres-Sempere [a], J.J. Villora-Picó [a], T.R. Reina [a,b,**], J.A. Odriozola [a,b]

[a] Inorganic Chemistry Department and Materials Sciences Institute, University of Seville-CSIC, Seville, Spain
[b] School of Chemistry & Chemical Engineering, University of Surrey, Guildford GU2 7XH, UK

ARTICLE INFO

Keywords:
Hydrothermal carbonization
Biomass
CO_2 waste valorization
Methanation
Ni-based catalyst
Circular economy

ABSTRACT

The utilization of biomass and bio-waste, particularly through hydrothermal processes, has shown promise as a technology for converting these materials into valuable products. While most research has traditionally focused on the solid and liquid byproducts of these hydrothermal treatments, the gaseous phase has often been overlooked. This study specifically investigates the conversion of off-gases produced during hydrothermal carbonation (HTC) into synthetic natural gas, offering a readily marketable product with economic potential. Although the methanation of conventional flue gases has been extensively studied, dealing with non-standard off-gases from processes like HTC presents challenges due to the presence of minor impurities like CO and CH_4. This novel research seeks to experimentally evaluate the methanation of HTC off-gases using nickel-based catalysts and analyze how these impurities affect the catalytic performance. The studied catalysts include nickel supported by ceria and alumina, as well as alumina supported nickel-cobalt systems. The results demonstrate that these catalysts exhibit high CO_2 conversion and CH_4 selectivity under ideal gas conditions. However, when real gas compositions with impurities are considered, CO_2 conversion decreases at lower temperatures (ca. 20% lower conversion for real gas vs. ideal), probably due to side reactions such as CH_4 cracking. This difference becomes less pronounced at higher temperatures. Nevertheless, the catalysts perform satisfactorily, especially at temperatures exceeding 350 °C. In conclusion, this study sheds light on the methanation of HTC off-gases and underscores the significance of understanding how impurities in real gases impact the process, providing potential directions for future research.

1. Introduction

1.1. Background

The continuous growth of the global population has led to an increase in energy demand, making it difficult for economies to maintain an equilibrium between energy demand and supply [1]. As fossil fuels become depleted, the transition to cleaner, renewable energy sources becomes crucial [2]. Biomass and bio-waste valorization have gained momentum as green sources to produce high-value products and renewable energy carriers [3,4]. Hydrothermal treatments are promising methods for transforming biomass and waste into valuable products [5]. Hydrothermal carbonization (HTC) leads to solid carbonaceous material, while hydrothermal liquefaction (HTL) and hydrothermal gasification (HTG) produce liquid and gaseous products, respectively [6]. Hydrochars obtained via HTC have a wide range of industrial applications, such as acting as a fossil coal substitute, adsorbent for toxic chemicals, energy storage material, and support of catalysts, among other purposes [6,7]. The liquid fraction of HTC can be used as co-substrate in anaerobic digestion or as fertilizer [8], while the gaseous phase has not been fully explored, despite its potential [9]. Previous studies showed that valorizing the HTC gaseous phase via the Reverse Water Gas Shift (RWGS) reaction is possible, producing a valuable syngas stream [10,11]. However, even with the market value of the produced syngas, the HTC route remains unprofitable [12]. Synthetic natural gas (SNG) offers an alternative ready-to-use product that can

* Corresponding author.
** Corresponding author at: School of Chemistry & Chemical Engineering, University of Surrey, Guildford GU2 7XH, UK.
E-mail addresses: jgonzalez15@us.es (J. González-Arias), tramirez@us.es (T.R. Reina).

https://doi.org/10.1016/j.jcou.2023.102653
Received 22 August 2023; Received in revised form 3 December 2023; Accepted 18 December 2023
Available online 21 December 2023

turn the process economic balance toward profitable scenarios [13]. The off-gas from HTC can be converted into methane via the methanation reaction, making it a proper feedstock for SNG. Even though the use of methanation for standard flue gases (composition of ca. 10–20% CO_2 and 80–90% N_2) is very well studied, the methanation of non-standards off-gases is still a challenge (i.e., how the minor impurities of the gas affect the overall catalytic performance) [14–16]. In this line, our team has previously performed an economic estimation to explore the profitability of combining HTC and methanation for SNG production [17]. One of the main conclusions of this work was that a technical improvement to improve cost performance is needed to reach profitable scenarios. In this sense, improving the utilization of off-gases coming from renewable-based processes is pivotal. Therefore, in this work an experimental evaluation of the performance of methanation of HTC off-gases is proposed. To this end, first an overview of methanation reaction is given, followed by a section in which the aim and scope is shown in order to understand the importance of this work.

1.2. Brief overview of methanation

Methanation is a chemical process that involves the conversion of CO_2 and H_2 into CH_4, following the reaction given in Eq. (1). Overall, the methanation process not only facilitates the production of methane but also represents a pivotal avenue for addressing key challenges associated with renewable energy storage and carbon dioxide emissions mitigation having the potential to play an important role in the transition to a low-carbon economy [18]. Methanation offers a unique solution by allowing to convert excess electricity generated during peak renewable energy production periods into methane, serving as a form of energy storage. This stored methane can later be utilized during periods of high energy demand or when renewable sources are less productive, thereby contributing to the overall stability and reliability of the energy grid [19]. Nonetheless, if carbon-based traditional fuels are to be used with less intensity over time, alternatives and renewable CO_2 sources will be needed (i.e., biogas or HTC off-gas). The integration of these alternative and renewable CO_2 sources into methanation processes aligns with the broader objective of achieving carbon neutrality and sustainability in energy systems.

$$CO_2 + 4H_2 \leftrightarrow CH_4 + 2H_2O \quad (1)$$

Methanation, a process pioneered by Sabatier and Senderens in 1902 [20], has undergone extensive investigation with various catalysts, including nickel-based, cobalt-based, ruthenium-based, and iron-based catalysts [21,22]. Among these, nickel-based catalysts have emerged as the most commercially utilized owing to their superior catalytic activity in methanation and cost-effective performance [21]. Given their prominence, much of the research in this domain has centered around nickel-based catalysts. This focus is driven by their demonstrated efficacy and potential to enhance the cost performance of targeted methanation processes.

The maximum yield of CH_4 occurs at a relatively low-temperature range of 300–400 °C (depending on reaction conditions), which results in less structural degradation of nickel-based catalysts compared to other reactions like methane dry reforming [23]. The choice of metal oxide support is also crucial in the performance of nickel-based catalysts, with Ni/CeO_2 catalysts exhibiting higher activity than Ni/Al_2O_3 or Ni/SiO_2 catalysts [23]. This is mainly attributed to ceria's unique redox and oxygen defect chemistry, which facilitates oxygen species and ion vacancy transportation throughout its lattice [24]. Ceria serves as a highly effective support material for nickel-based catalysts in CO_2 methanation, primarily due to its higher basicity. This characteristic enhances the chemisorption and activation of CO_2 molecules, crucial for efficient conversion to methane. Furthermore, the strong metal-support interaction (SMSI) of ceria ensures a stable catalyst structure, preventing sintering of nickel particles and promoting a high dispersion of active sites. These attributes collectively contribute to the superior catalytic performance, prolonged catalyst life, and enhanced efficiency of ceria-supported catalysts in the methanation process, making them a preferred choice for CO_2 conversion to methane [25].

Incorporating a second metal as a promoter into nickel-based catalysts is a viable method for achieving desirable catalytic performance [26]. The introduction of a second metal may lead to the formation of an alloy structure with nickel, thereby modifying the geometric and electronic properties of the nickel-based catalysts. Literature suggests that potential promoters include alkaline earth oxides, noble metals, rare-earth metals, and other transition metals and non-metallic elements, see for example references [27–33]. The promoters can impact the dispersion of nickel active sites, the acid-base properties of the support, the nickel-support interaction, and ultimately the catalytic activity and stability of the catalyst [34]. Among active metal promoters, cobalt shows good manufacturing costs and technical performance [32,35]. In fact, nickel-cobalt catalysts have been deeply studied for CO_2 methanation [36].

Researchers have traditionally focused their efforts on the catalyst configurations to maximize catalytic activity and stability. This includes the design of multifunctional catalysts, core-shell structures, and catalysts with tailored surface properties to optimize the distribution of active sites and improve resistance to deactivation [37,38]. However, the exploration of emerging trends in methanation research encompasses a spectrum of innovative approaches, from advanced reactor designs and computational modeling to real-time monitoring and integration with renewable feedstocks, collectively advancing the field towards more sustainable and efficient methane production. In this sense, researchers are actively exploring novel reactor designs to enhance the efficiency of methanation processes. This includes the investigation of advanced reactor configurations, such as membrane reactors, fluidized bed reactors, and microreactors [39–41]. These designs aim to optimize mass and heat transfer, providing better control over reaction conditions and improving overall performance. Similarly, techniques such as microwave-assisted methanation and plasma-assisted catalysis are gaining attention for their potential to enhance reaction rates and selectivity [42–45]. These strategies offer opportunities to streamline methanation processes and make them more energy efficient.

The utilization of advanced computational modeling tools is also becoming increasingly prevalent in methanation research. Computational approaches, including machine learning techniques, aid in predicting catalyst behavior, optimizing reaction conditions, and accelerating the discovery of new catalytic materials [46,47]. This trend holds promise for accelerating the development of efficient methanation processes.

1.3. Aim and scope

The trend of integrating methanation with renewable feedstocks is booming. Investigating the use of biomass-derived syngas, biogas, and other renewable sources as feedstocks for methanation is currently gaining momentum [48–50]. This approach aligns with the broader goal of utilizing sustainable resources for methane production, contributing to the overall decarbonization of the process. In line with these challenges, in this work an experimental investigation into the methanation of HTC off-gases is proposed. The novelty of this work lies in this experimental study. We aim to evaluate the catalytic performance of this process considering the impact of impurities present in the off-gases. Fig. 1 shows a scheme of the process idea. The focus on methanation of HTC off-gases is innovative, as it addresses a challenging aspect of the process, particularly in understanding how the minor impurities affect catalytic performance. Impact of impurities is often disregarded in academic studies but essential for real-world applications. Hence, this work contributes to the broader goal of developing economically viable synthetic natural gas (SNG) production from HTC off-gases, offering valuable insights into the optimization of catalytic processes for renewable energy generation. The selection of two specific nickel-based

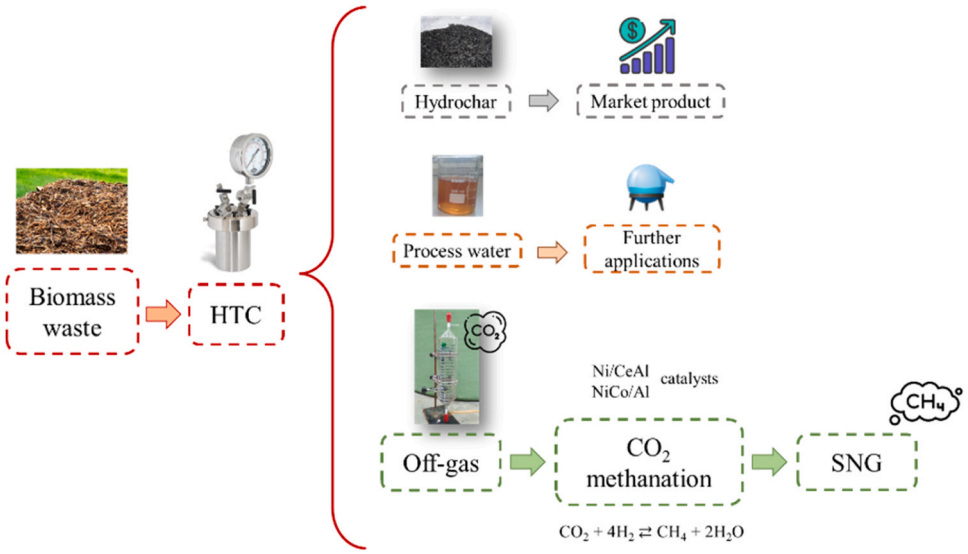

Fig. 1. Process idea scheme.

catalysts: (1) nickel supported over ceria and alumina (Ni/CeAl from now on); and (2) nickel-cobalt supported over alumina (NiCo/Al from now on), adds further novelty to the research, allowing for a comparative study on the influence of the active phase and support in the catalytic conversion of HTC off-gases. In addition, this research aims to maximize the value derived from the entire HTC process, including the gaseous byproducts, making it more sustainable and economically viable.

The paper is structured as follows: first a description of the materials and methods, including physicochemical characterization of the catalysts is shown. Then investigation on the impact of impurities on catalytic activity by comparing "ideal gas" (typical standard flue gas) and "real gas" (representing common minor impurities found in HTC off-gases (CO and CH_4) [10]) is presented. The catalytic activity is assessed through conversion and selectivity measurements, and potential reaction mechanisms are discussed. Finally, conclusions and suggestions for future research are presented.

2. Materials and methods

2.1. Catalyst preparation

The co-impregnation method was utilized to synthesize the catalysts. For the NiCo/Al catalyst, to obtain a 15 wt% of Ni and 3.5 wt% of Co on commercial Al_2O_3 SASOL (Alumina Puralox Scca 30/200), the required amount of $Ni(NO_3)_2$-6 H_2O and $Co(NO_3)_2$ 6 H_2O was added. For the Ni/CeAl, the exact amount of $Ni(NO_3)_2$-6 H_2O was added to the commercial CeO_2/Al_2O_3 support (Puralox SCFA 160/ Ce 20 Sasol CeO_2/Al_2O_3) to obtain a 15 wt% of Ni. Following the impregnation, the excess solvent was evaporated, and the samples were dried overnight at 110 °C. Finally, both samples were calcinated at a rate of 5 °C/min, reaching 400 °C for 4 h.

2.2. Characterization techniques

X-ray diffraction (XRD) analysis was performed over the calcined samples to verify the formation of oxides. X-ray diffraction measurements were performed using an X'Pert Pro PANalytic instrument with Cu-Kα radiation (λ = 0.154 nm) at 40 mA and 45 kV. The diffraction patterns were recorded in a range of 10 to 90° using a step size of 0.05° and a step time of 300 s

Temperature-programmed reduction (TPR) measurements were conducted using a conventional U-shaped quartz reactor connected to a thermal conductivity detector (TCD). A flow of 50 mL/min of 5% H_2 diluted in Ar and approximately 50 mg of each catalyst were used for the TPR measurements. The heating rate was 10 °C/min from room temperature to 900 °C. To remove the water formed during the procedure, a mixture of acetone and dry ice was used as a cold trap.

X-ray photoelectron spectroscopy (XPS) experiments were conducted using a SPECS photoelectron spectrometer, which was equipped with a PHOIBOS 150 MCD analyzer. The analyzer operated with a constant pass energy of 40 eV and a resolution of 1.0 eV. For the X-ray radiation source, we utilized the Kα emission generated by bombarding an aluminum target with electrons, resulting in X-rays with an energy of hν = 1486.6 eV and a bandwidth of 0.85 eV. This source operated at 250 W and maintained a potential of 12.5 kV. The analysis chamber operated in an ultra-high vacuum environment, maintaining a pressure of 10^{-10} mbar.

2.3. Catalytic activity tests

The catalytic activity was assessed in a fixed-bed continuous-flow reactor, as described in reference [51]. For each run, 200 mg of undiluted catalyst was loaded and in situ reduced in a flow of 10% H_2 and 90% N_2 at 650 °C for 1 h before the reaction. The WHSV (Weight Hourly Space Velocity) was maintained at 30 L/g_{cat}·h. For the ideal gas tests, gas mixtures were created with a composition of 15% CO_2, 60% H_2, and N_2 balanced. For real gas coming from HTC, the feed stream was prepared with a composition of 15% CO_2, 60% H_2, 1% CO, and 1% CH_4 (N_2 balanced), replicating the gaseous product generated in the HTC thermal process, as per the results obtained in a previous study [52]. To achieve this composition, we made necessary adjustments to the gas supply. Given that we followed the methanation reaction (Eq. (1)) and based on the stoichiometry of the reaction, a CO_2/H_2 ratio of 4 was chosen. As such, CO and CH_4 were set at 1%, considering the limitations of mass flow controllers. With these settings, CO_2 corresponded to approximately 15% of the total gas composition. It is important to note that the H_2 produced during the HTC process, as abovementioned, was in trace amounts, necessitating an external hydrogen supply. Hence, we supplied 60% H_2, in accordance with the CO_2/H_2 ratio mentioned earlier. The composition of the inlet and outlet gas flows was measured with an ABB analyzer equipped with Caldos 25 and Uras 36 housing units. The reaction was evaluated at a temperature range of 200–450 °C, in agreement with previous studies for methanation [41,53–55]. It is important to emphasize that the testing duration at each temperature point, which was approximately 40 min, was subject to slight variations to ensure the

achievement of a stable and consistent operating condition. This variation in testing time was necessary to guarantee the reliability and accuracy of the experimental results by allowing the process to reach a steady state. The catalytic results (CO_2 conversion and CH_4 selectivity) were expressed according to Eqs. (2)–(3):

$$CO_2 \quad conversion = \frac{CO_{2,in} - CO_{2,out}}{CO_{2,in}} x100 \tag{2}$$

$$CH_4 \quad selectivity = \frac{CH_{4,out}}{CO_{2,in} - CO_{2,out}} x100 \tag{3}$$

3. Results and discussion

The first step was the characterization of the catalysts prepared. Even though the focus of the paper is to analyze the impact of minor impurities (e.g., CO and CH_4) on the methanation activity, a minor physicochemical characterization is needed to verify the formation of the oxides in the catalysts and to know the reduction temperature needed for the reaction. XRD technique was used to analyze the structure of both prepared catalysts. The samples were analyzed after calcination at 400 °C (Fig. 2). As shown in the figure, all samples exhibited the characteristic diffraction lines of the Al_2O_3 phase (00–004-0858), see for example peaks at ca. 37° and 66° [51]. The spinel-like peaks of the $NiAl_2O_4$ (00–010-0339) and $CoAl_2O_4$ (00–038-0814) phases can also be observed in the diffractogram, indicating a strong interaction of the active phases within the support [56–58]. NiO peaks (00–047-1049) were also found [51,59], verifying the formation of the oxide species. The characteristics peaks of CeO_2 (00–004-0593) can be seen in the diffractogram of the Ni/CeAl catalyst [60].

Fig. 3 shows the H_2-TPR profiles displayed by the catalysts used. The profile for the NiCo/Al catalyst shows a reduction peak at 278 °C, which is associated with the reduction of Co_3O_4 into CoO [61]. Moreover, a broad band with two shoulders at about 466 and 552 °C appears. These shoulders can be attributed to the reduction of CoO into metallic Co^0 and to the reduction of NiO, respectively [62]. Certainly, in several studies it was proposed that the reducibility of Ni and Co species was enhanced simultaneously in supported NiCo catalysts [63]. The small shoulder at ca. 780 °C shows the presence of hardly reducible species of Ni attributed to the presence of the spinel $NiAl_2O_4$ [64]. Concerning the Ni/CeAl catalysts, NiO reduction is observed at ca. 306 °C which is assigned to the reduction of superficial NiO. This relatively lower reduction temperature is the result of the interaction with the CeO_2 support [65]. The broad band which appears between 400–700 °C reveals two peaks (407 and 520 °C) associated with the reduction of NiO and with the reduction of superficial ceria promoted by the metallic nickel formed, respectively [66]. Furthermore, as in the NiCo/Al, a small peak is observed at 786 °C related with the reduction of the $NiAl_2O_4$ spinel [67].

The surface chemistry assessment of the prepared materials, both prior to and after the reduction treatment, was conducted through XPS

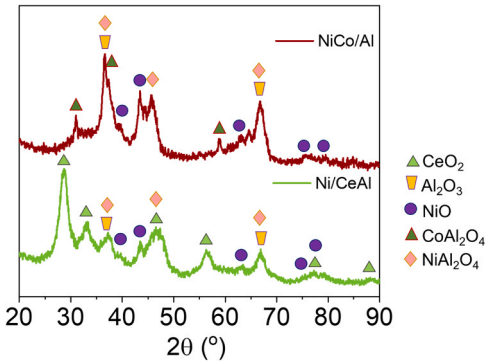

Fig. 2. XRD diffractograms exhibited by calcined catalysts.

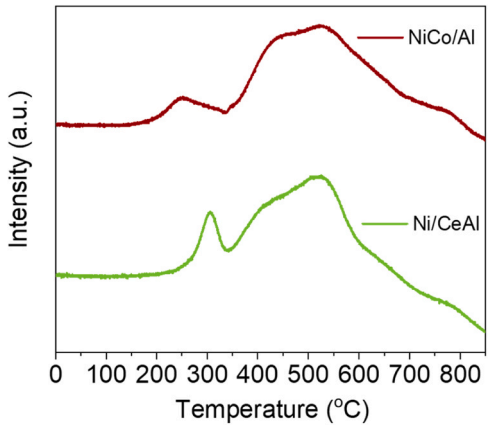

Fig. 3. H_2-TPR profiles for the calcined catalysts.

to elucidate the impact of this process on the materials under investigation. Examination of the Ni 2p spectrum (Fig. 4) reveals the emergence of two principal peaks at 850.5 eV and 854.4 eV, corresponding to Ni^0 and Ni^{2+}, respectively [68]. As anticipated, a substantial reduction in the quantity of Ni^{2+} is evident post-reduction, indicative of a considerable conversion to metallic Ni. The atomic composition of the surface, as determined by XPS and presented in Table 1, illustrates a noteworthy decrease in surface Ni content following the reduction treatment. This phenomenon suggests potential sintering of metallic particles, leading to a diminished presence of Ni on the surface, corroborated by an augmented concentration of Al on the surface.

In the case of the catalyst incorporating Ce, the sintering effect is accompanied by a potential Strong Metal-Support Interaction (SMSI) phenomenon, wherein a portion of the Ni nanoparticles becomes coated by migrating Ce from the support, as evidenced by a substantial decrease

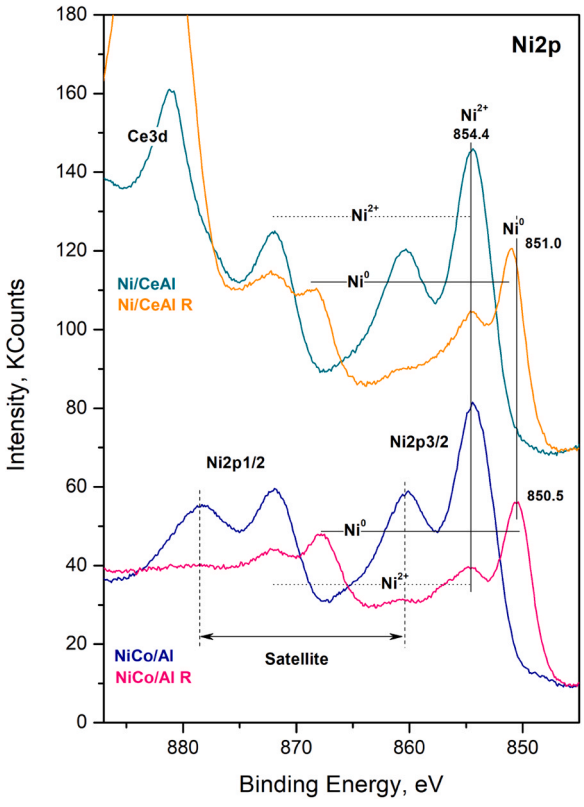

Fig. 4. Ni 2p XPS spectrum for the Ni/CeAl and the NiCo/Al catalysts before, and after reduction (R).

Table 1
Atomic composition of the surface for both catalysts before and after reduction (RED).

% at	C	O	Al	Al/O	Ni	Co	Ce
NiCo/Al	4.0	57.2	34.1	0.60	4.6	0.16	-
Ni/CeAl	6.1	55.8	29.5	0.53	6.1	-	2.5
Ni/CoAl RED	0.9	59.8	37.4	0.62	1.8	0.16	-
Ni/CeAl RED	0.5	59.4	33.2	0.56	2.8	-	4.1

in surface Ni content [69,70]. Notably, the peak corresponding to metallic Ni in the Ce-containing sample shifts to higher binding energies (851 eV), indicating a reduced electron density, possibly attributed to Ce-induced electron density reduction. This inference is supported by an elevated Ce concentration on the catalyst surface, increasing from 2.5 to 4.1 at. percent. The Ce 3d spectrum (Fig. 5) exhibits characteristic peaks associated with CeO_2, with the fresh sample displaying distinct Ce^{4+} peaks (V1, V2, V3, V4, V5, and V6). However, post-reduction treatment, a reduction of Ce^{4+} to Ce^{3+} is observed, evidenced by the diminished Ce^{4+} peaks and the emergence of two new peaks (U1 and U2) corresponding to Ce^{3+} [71].

Analysis of the Co 2p spectrum (Fig. 6) prior to reduction reveals a singular peak at 780.1 eV, indicative of Co^{2+} presence. Subsequent to the reduction treatment, a new peak emerges at 776.7 eV, corresponding to Co^0, signifying the reduction of a portion of Co. Importantly, the reduction treatment does not impact the overall quantity of Co, suggesting that there is no discernible sintering of Co particles, which remain strongly bound to the support.

Fig. 7 depicts the catalytic activity shown by NiCo/Al as a function of temperature. This evaluation is carried out for both ideal and real gas conditions. This comparison allows us to discern and evaluate the specific impact of these trace impurities on the catalyst's deactivation right from the reaction kick-off. While side reactions leading to the production of CO and CH_4 may occur at higher temperatures, understanding the initial impact of these impurities is fundamental for a comprehensive

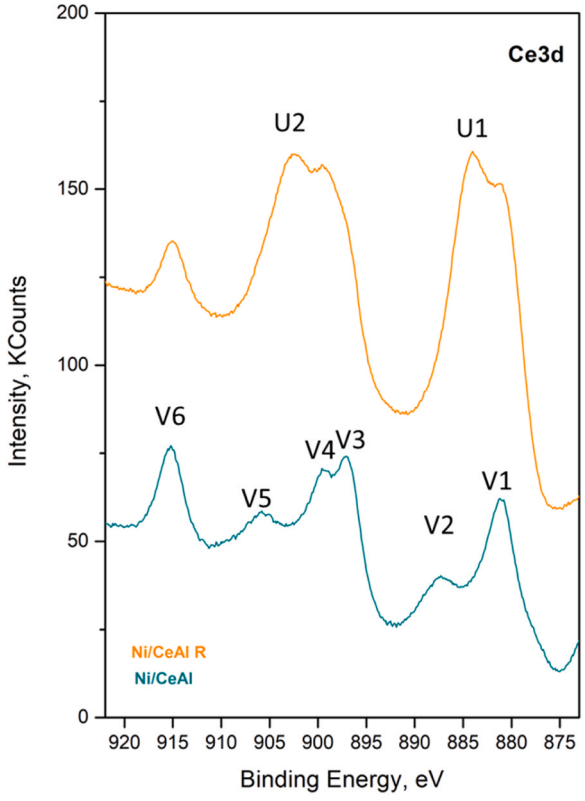

Fig. 5. Ce 3d spectrum for the Ni/CeAl catalyst before and after reduction (R).

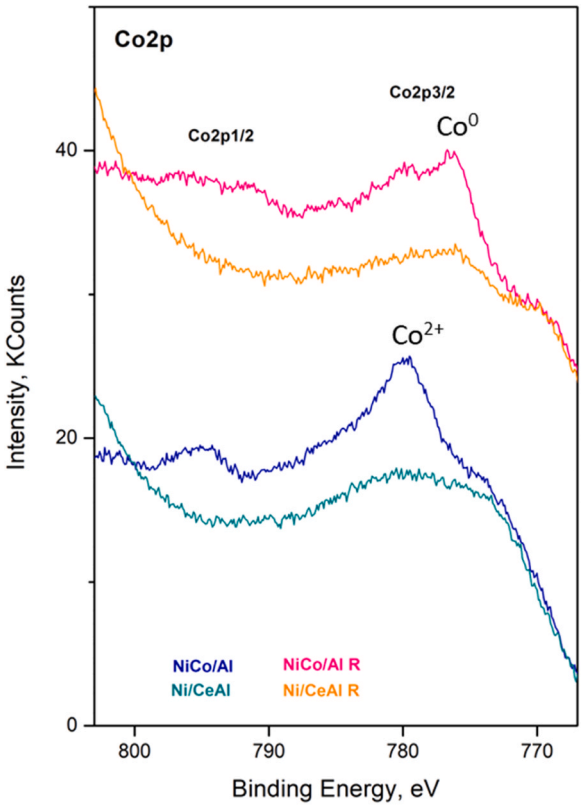

Fig. 6. Co 2p XPS spectrum for both Ni/CeAl and NiCo/Al catalysts before, and after reduction (R).

assessment of the catalyst's performance and durability. By studying the catalyst's behavior in an idealized environment, we establish a baseline for its expected performance. Beginning with the results obtained at ideal conditions, the performance of our catalyst falls into the range of conversions obtained in previous works for nickel- and cobalt-based catalysts [35,72–75]. Although it might be surprising to find a CO_2 conversion value of 70–80% at 250–350 °C, this result is in line with previous works for medium-high loads of metal in the catalyst [35,72]. In fact, the presence of cobalt seems to highly favor the conversion [35]. The comparison between our catalysts and previous similar works for ideal conditions can be seen in Table 2. Nevertheless, the CO_2 conversion obtained drops dramatically at low temperatures (250–300 °C) in the case of real gas composition, as expected by thermodynamics when including minor impurities (CO and CH_4), and for the kinetics of the reaction at these temperatures. For example, there was a loss of ca. 20% conversion at 250 °C. This difference gets lower at higher temperatures, having the minimum at 450 °C (69% ideal gas vs. 63% real gas). The reason behind this fact is a combination of side reactions caused by minor impurities. At relatively low temperatures (250–300 °C), there is a possibility of CH_4 cracking (Eq. (4)) or the water-gas shift (WGS) (Eq. (5)) reactions occurring to some degree [76,77]. While methane cracking is inherently endothermic, it has been observed to occur within the specified operating range, as documented elsewhere [78]. Additionally, within this temperature range, there is a potential for the reconversion of carbon to CO_2 through the utilization of water generated in the methanation reaction (Eq. (6)). This reaction plays a crucial role in gasifying any potential carbon deposits resulting from methane cracking, thereby preventing deactivation [79]. This reaction results in the formation of C and H_2. The presence of C can potentially obstruct the active sites of the NiCo/Al catalyst, leading to a decrease in the conversion of CO_2. However, at elevated temperatures, the formed C may undergo oxidation in the presence of a catalyst, resulting in the production of more CO or CO_2. These byproducts can then participate in

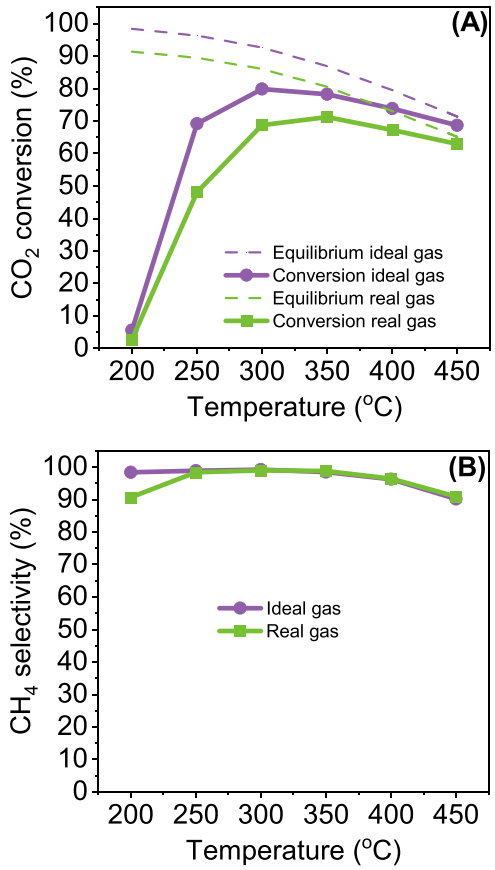

Fig. 7. Catalytic activity exhibited by NiCo/Al: (A) CO_2 conversion; (B) CH_4 selectivity.

Table 2
Comparison of NiCo/Al vs. previous works with relatively similar conditions for ideal gas composition (i.e., without minor impurities).

Catalyst	H_2/CO_2 ratio	WHSW (L/g•h)	Temperature (°C)	Specific rate CO_2 (L/g·h) *	Reference
25% Ni/Al_2O_3	4	11.4	300	0.912	[35]
15% Co/Al_2O_3	4	11.4	300	1.824	[35]
15% Ni – 5% Co/Al_2O_3	4	13	300	2.002	[72]
15% Ni/Al_2O_3	4	13	300	2.158	[72]
15% Ni – 3.5% Co/Al_2O_3	4	30	300	4.740	This work

* Calculated considering 20% CO_2 and 80% H_2.

further reactions, sustaining the production of CH_4. This observation clarifies the smaller discrepancy observed at higher temperatures between the behavior of ideal gases and real gases. In any case, the results obtained from 350 °C are fairly close to equilibrium, displaying a quite acceptable performance even for real conditions with minor impurities.

$$CH_4 \leftrightarrow C + 2H_2 \quad (4)$$

$$CO + H_2O \leftrightarrow CO_2 + H_2 \quad (5)$$

$$C + 2H_2O \leftrightarrow CO_2 + 2H_2 \quad (6)$$

Concerning CH_4 selectivity, the results obtained for ideal gas are always higher than 90% and very close to 100% in most of the cases, revealing a high selectivity of NiCo/Al towards CH_4 and minimizing CO production. At the highest temperature tested, CH_4 selectivity slightly drops which can be a symptom of the presence of the reverse water gas shift (RWGS) reaction (Eq. (7)) [80]. As for the real gas composition, an analogous behavior is observed for CH_4 selectivity except for the first point of the temperature series. This might be caused by the rather low CO methanation at low temperatures [81,82], entailing a higher CO presence at the outlet and hence a lower CH_4 selectivity result.

$$CO + H_2O \leftrightarrow CO_2 + H_2 \quad (7)$$

This assumption can also be explained because at temperatures below 400–450 °C, the reduction of CO_2 through Eq. (8) does not occur. However, at elevated temperatures (above 450 °C), this reduction might take place as methane selectivity decreases, leading to an increased preference for CO [79].

$$CO_2 + C \leftrightarrow 2CO \quad (8)$$

An additional reaction that could impact the results is the Boudouard reaction, resulting from the production of CO and potentially leading to carbon deposition on the catalyst. Nevertheless, given the complexity of the various reactions that may occur in this context, we cannot confirm the presence of the Boudouard reaction. We acknowledge the imperative for future research endeavors to delve deeper into the exploration of potential side reactions. Validating the presence of side reactions is beyond the scope of this paper which is conceived as a proof-of-concept for the methanation reaction under surrogate HTC off-gases. Future works should aim to bridge the gaps left by our constraints, contributing to a deeper exploration of side reactions in the context of the methanation of HTC off-gases.

The results presented clearly demonstrate that the presence of these impurities does affect the overall performance of the reaction, despite their common occurrence in methanation. The reduction in performance when a simulated real gas stream is used underscores the importance of considering these impurities in practical applications. This insight is invaluable for the design and optimization of catalysts in real-world scenarios, where gas streams may not be as pure as in idealized laboratory conditions.

Fig. 8 showcases the results obtained for the catalytic activity of Ni/CeAl for different temperatures. In this case, the CO_2 conversion is quite high even at 200 °C (ca. 50% for both ideal and real conditions). This is a remarkable result since working at 200 °C would entail considerable energy and economic savings. On the other hand, separation costs would increase since there would be a higher share of unreacted raw gases in the gas outlet. This would require a full technical optimization and economic analysis, as proposed elsewhere [17]. But let's focus now on the high CO_2 conversion obtained. The reason behind is the remarkable impact of the ceria for methanation at low temperatures. Indeed, this fact has been previously studied in some works [83–86]. This high effect of ceria for Ni/Al_2O_3 catalyst seems to be that ceria addition favors the dispersion of NiO species and increases the metal-support interaction [83]. Furthermore, by incorporating CeO_2 into the catalyst formulation, the acidity of the Al_2O_3 support is diminished, and the oxygen mobility is enhanced. These two factors play a crucial role in preventing the deposition of carbon. Oxidation and/or gasification of the carbonaceous species is favored due to the redox properties of ceria [67,87]. Likewise, the addition of ceria seems to improve the reducibility of the catalyst [88]. This is confirmed in our TPR analysis shown in Fig. 3. All in all, it seems reasonable to conclude that the use of ceria is advisable for low temperature methanation even for real gas compositions. As for the rest of the temperatures shown in Fig. 8, the trend is very similar to the one shown by NiCo/Al_2O_3 catalysts with slightly lower impact from the real gas conditions, hence equivalent conclusions can be drawn. Regarding CH_4 selectivity, the result obtained is very high as in the previous catalyst tested. This result is also in line with previous works which used ceria as a promoter for alumina catalysts [83].

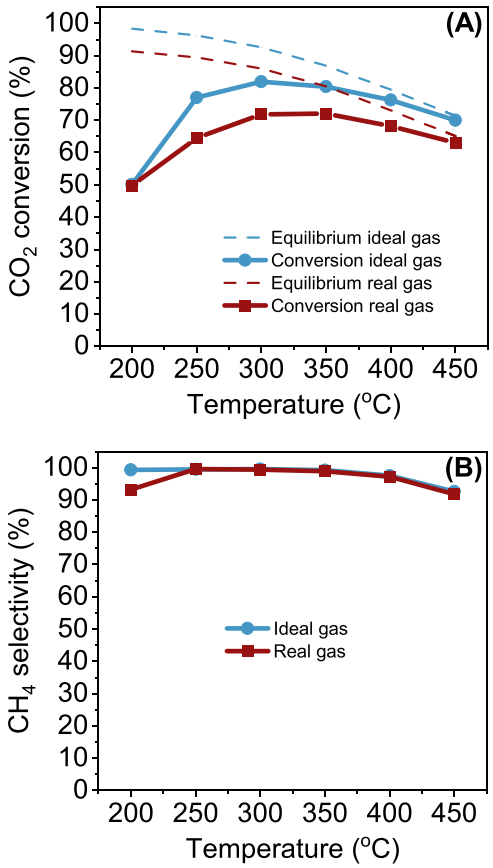

Fig. 8. Catalytic activity exhibited by Ni/CeAl: (A) CO_2 conversion; (B) CH_4 selectivity.

Digging a bit more into the results obtained for both catalysts, Fig. 9 shows a comparison of the CO_2 conversion for real gas compositions. The first and most evident conclusion is that we can strongly suggest the use of ceria instead of cobalt for the low-temperature range (200–250 °C), while at higher temperatures the conversions are similar. The reason for this might be related to the explanation given above for CH_4 cracking and the positive effect of ceria avoiding carbon deposition due to the acidity reduction of the support. In the case of the Ce-supported catalyst the conversion under real gas conditions might be higher because Ce reduces quite well at low temperatures. This reduction provokes a faster oxidation of the C formed by Eq. (4), with a consequent CH_4 formation. This hypothesis would also agree with the results obtained at higher temperatures for the same explanation given before.

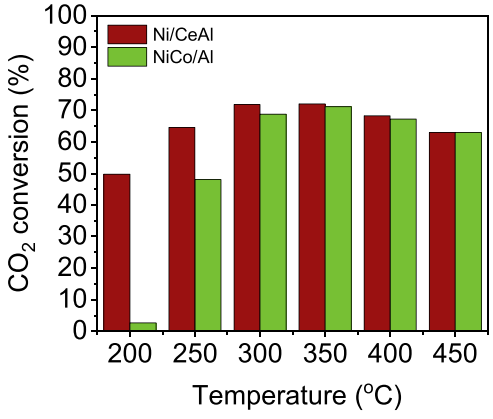

Fig. 9. Comparison between Ni/CeAl vs. NiCo/Al for real gas composition.

The last step was the characterization of the catalysts used to check the potential differences in the XRD between ideal and real conditions. The results obtained are represented in Figs. 10 and 11 for the NiCo/Al and Ni/CeAl catalysts, respectively. As shown, and in contrast with the catalytic activity results, there are no differences between ideal and real conditions, meaning that the minor impurities of HTC off-gases do not affect the overall crystallinity of the catalysts. In comparison with the pre-used catalyst diffractogram, in the used ones we can see metallic nickel (Figs. 10 and 11), which agrees with the methanation reaction since hydrogen consumption reduces oxides. In the NiCo/Al catalyst, a Ni-Co alloy is formed, shifting the metallic Ni peaks to higher angles.

4. Conclusions

This study focused on the experimental evaluation of HTC off-gases methanation using nickel-based catalysts. The aim of this work was to investigate the effect of impurities on the catalytic activity by comparing two catalysts, NiCo/Al and Ni/CeAl. The XRD analysis confirmed the formation of the desired oxide species in the catalysts, while the TPR profiles provided insights into the reduction behavior of the catalysts. Catalytic activity tests were conducted using a fixed-bed continuous-flow reactor. The catalytic performance was evaluated under ideal gas conditions and real gas conditions, simulating the composition of HTC off-gases with minor impurities. The catalytic activity results revealed significant differences among ideal and real gas conditions. NiCo/Al exhibited high CO_2 conversion and CH_4 selectivity under ideal conditions, aligning with previous works for similar bimetallic catalysts. However, when subjected to real gas conditions, a notable reduction in CO_2 conversion was observed at lower temperatures (ca. 20% lower conversion for real gas vs. ideal), attributed to side reactions, particularly CH_4 cracking. Despite this, the catalyst demonstrated acceptable performance at higher temperatures, emphasizing its resilience to real gas compositions. Ni/CeAl, on the other hand, displayed remarkable CO_2 conversion even at 200 °C, suggesting the potential for energy and economic savings. The high impact of ceria on methanation at low temperatures was evident, attributed to its ability to enhance metal dispersion, reduce acidity, and improve catalyst reducibility. The CH_4 selectivity results were consistently high, in line with the positive influence of ceria as a promoter. Comparative analysis between the two catalysts for real gas conditions indicated a strong recommendation for the use of ceria instead of cobalt at low temperatures (200–250 °C), with comparable performance at higher temperatures. Further XRD characterization demonstrated no significant differences between ideal and real gas conditions, indicating that minor impurities in HTC off-gases did not affect the overall crystalline structure of the catalysts.

The study provides valuable insights into the methanation of HTC off-gases and highlights the challenges associated with the presence of minor impurities. There are shreds of evidence that the minor impurities affect considerably the overall performance. Moreover, the results

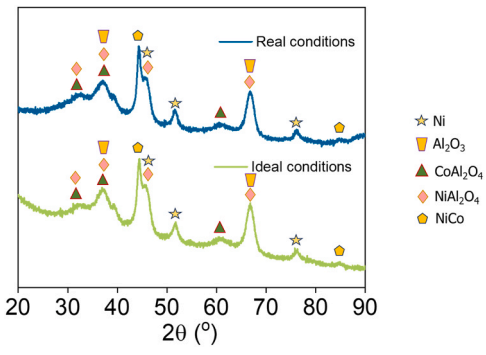

Fig. 10. XRD diffractograms exhibited by the used NiCo/Al catalysts.

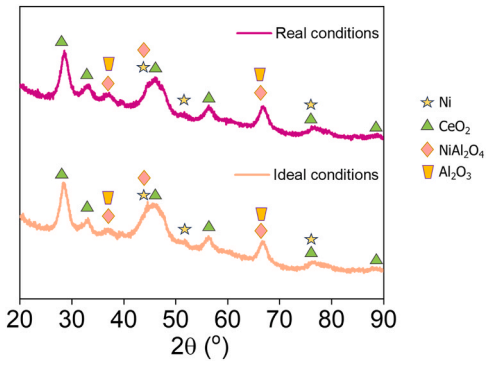

Fig. 11. XRD diffractograms exhibited by used Ni/CeAl catalysts.

contribute to the understanding of catalytic reactions in the context of renewable energy and offer possibilities for further improvements in the utilization of off-gases from renewable-based processes. Future research directions may include exploring alternative catalyst formulations, optimizing reaction conditions, and investigating the mechanism of side reactions to enhance the performance and economic viability of the methanation process for SNG production. The findings underscore the potential of renewable CO_2 sources and provide valuable insights for the development of efficient and cost-effective processes for SNG production.

CRediT authorship contribution statement

J. González-Arias: Conceptualization; Formal analysis; Investigation; Writing – original draft; Writing – review & editing. **G. Torres-Sempere:** Data curation; Formal analysis. **J.J. Villora-Picó:** Data curation; Formal analysis; Methodology. **T.R. Reina:** Conceptualization; Funding acquisition; Project administration; Writing – original draft; Writing – review & editing. **J.A. Odriozola:** Project administration; Resources; Supervision; Writing – review & editing.

Declaration of Competing Interest

The authors declare that they have no known competing financial interests or personal relationships that could have appeared to influence the work reported in this paper.

Data availability

Data will be made available on request.

Acknowledgments

This work has been supported by the FJC2021–047672-I grant co-financed by MCIN/AEI/10.13039/501100011033 and the European Union NextGenerationEU/PRTR funds. This work was also partially sponsored by Spanish Ministry of Science and Innovation through the projects PLEC2021–008086 sponsored by MCIN/AEI/10.13039/501100011033 Next Generation Europe and PID2021–126876OB-I00. This work was also partially sponsored by European Commission through the H2020-MSCARISE-2020 BIOALL project (Grant Agreement: 101008058).

References

[1] M. Xu, M. Yang, H. Sun, M. Gao, Q. Wang, C. Wu, Bioconversion of biowaste into renewable energy and resources: a sustainable strategy, Environ. Res 214 (2022), https://doi.org/10.1016/j.envres.2022.113929.

[2] F.M. Baena-Moreno, E. Le Saché, C.A. Hurd Price, T.R. Reina, B. Navarrete, From biogas upgrading to CO2utilization and waste recycling: a novel circular economy approach, J. CO_2 Util. 47 (2021), https://doi.org/10.1016/j.jcou.2021.101496.

[3] M. González-Castaño, M.H. Kour, J. González-Arias, F.M. Baena-Moreno, H. Arellano-Garcia, Promoting bioeconomy routes: From food waste to green biomethane. A profitability analysis based on a real case study in eastern Germany, J. Environ. Manag. 300 (2021), https://doi.org/10.1016/j.jenvman.2021.113788.

[4] J. González-Arias, E.J. Martínez, X. Gómez, M.E. Sánchez, J. Cara-Jiménez, Enhancing biomethane production by biochar addition during anaerobic digestion is economically unprofitable, Environ. Chem. Lett. 20 (2022), https://doi.org/10.1007/s10311-021-01368-8.

[5] J. González-Arias, M.E. Sánchez, J. Cara-Jiménez, Profitability analysis of thermochemical processes for biomass-waste valorization: a comparison of dry vs wet treatments, Sci. Total Environ. 811 (2022), https://doi.org/10.1016/j.scitotenv.2021.152240.

[6] J. González-Arias, M.E. Sánchez, J. Cara-Jiménez, F.M. Baena-Moreno, Z. Zhang, Hydrothermal carbonization of biomass and waste: a review, Environ. Chem. Lett. 20 (2022), https://doi.org/10.1007/s10311-021-01311-x.

[7] A. Parra-Marfíl, R. Ocampo-Pérez, V.H. Collins-Martínez, L.M. Flores-Vélez, R. Gonzalez-Garcia, N.A. Medellín-Castillo, G.J. Labrada-Delgado, Synthesis and characterization of hydrochar from industrial Capsicum annuum seeds and its application for the adsorptive removal of methylene blue from water, Environ. Res 184 (2020), https://doi.org/10.1016/j.envres.2020.109334.

[8] J. González-Arias, M.A. de la Rubia, M.E. Sánchez, X. Gómez, J. Cara-Jiménez, E. J. Martínez, Treatment of hydrothermal carbonization process water by electrochemical oxidation: assessment of process performance, Environ. Res 216 (2023), 114773, https://doi.org/10.1016/J.ENVRES.2022.114773.

[9] J. González-Arias, F.M. Baena-Moreno, M.E. Sánchez, J. Cara-Jiménez, Optimizing hydrothermal carbonization of olive tree pruning: a techno-economic analysis based on experimental results, Sci. Total Environ. 784 (2021), https://doi.org/10.1016/j.scitotenv.2021.147169.

[10] J. González-Arias, M. González-Castaño, M.E. Sánchez, J. Cara-Jiménez, H. Arellano-García, Valorization of biomass-derived CO_2 residues with Cu-MnOx catalysts for RWGS reaction, Renew. Energy 182 (2022), https://doi.org/10.1016/j.renene.2021.10.029.

[11] M. González-Castaño, J. González-Arias, M.E. Sánchez, J. Cara-Jiménez, H. Arellano-García, Syngas production using CO_2-rich residues: from ideal to real operating conditions, J. CO_2 Util. 52 (2021), https://doi.org/10.1016/j.jcou.2021.101661.

[12] J. González-Arias, F.M. Baena-Moreno, M. González-Castaño, H. Arellano-García, Economic approach for CO_2 valorization from hydrothermal carbonization gaseous streams via reverse water-gas shift reaction, Fuel 313 (2022), https://doi.org/10.1016/j.fuel.2021.123055.

[13] J. Beyrami, M. Jalili, M. Ziyaei, A. Chitsaz, M.A. Rosen, A novel system for electricity and synthetic natural gas production from captured CO_2: techno-economic evaluation and multi-objective optimization, J. CO_2 Util. 63 (2022), https://doi.org/10.1016/j.jcou.2022.102116.

[14] G.E. de Araujo, J.H. de Castro, W.F. Monteiro, J. de Lima, R.A. Ligabue, R. V. Lourega, Methanation of CO_2 from flue gas: experimental study on the impact of pollutants, React. Kinet., Mech. Catal. 134 (2021), https://doi.org/10.1007/s11144-021-02092-8.

[15] K. Müller, M. Fleige, F. Rachow, D. Schmeißer, Sabatier based CO_2-methanation of flue gas emitted by conventional power plants, : Energy Procedia (2013), https://doi.org/10.1016/j.egypro.2013.08.028.

[16] S. Morimoto, N. Kitagawa, N. Thuy, A. Ozawa, R.A. Rustandi, S. Kataoka, Scenario assessment of implementing methanation considering economic feasibility and regional characteristics, J. CO_2 Util. 58 (2022), https://doi.org/10.1016/j.jcou.2022.101935.

[17] J. González-Arias, G. Torres-Sempere, M. González-Castaño, F.M. Baena-Moreno, T.R. Reina, Hydrochar and synthetic natural gas co-production for a full circular economy implementation via hydrothermal carbonization and methanation: an economic approach, J. Environ. Sci. (2023), https://doi.org/10.1016/J.JES.2023.04.019.

[18] W. Gac, W. Zawadzki, M. Kuśmierz, G. Słowik, W. Grudziński, Neodymium promoted ceria and alumina supported nickel catalysts for CO_2 methanation reaction, Appl. Surf. Sci. 631 (2023), 157542, https://doi.org/10.1016/J.APSUSC.2023.157542.

[19] T. Schaaf, J. Grünig, M.R. Schuster, T. Rothenfluh, A. Orth, Methanation of CO_2 - storage of renewable energy in a gas distribution system, Energy Sustain Soc. 4 (2014), https://doi.org/10.1186/s13705-014-0029-1.

[20] D. Schmider, L. Maier, O. Deutschmann, Reaction kinetics of CO and CO2Methanation over Nickel, Ind. Eng. Chem. Res 60 (2021), https://doi.org/10.1021/acs.iecr.1c00389.

[21] S. Rönsch, J. Schneider, S. Matthischke, M. Schlüter, M. Götz, J. Lefebvre, P. Prabhakaran, S. Bajohr, Review on methanation - from fundamentals to current projects, Fuel 166 (2016), https://doi.org/10.1016/j.fuel.2015.10.111.

[22] S. Biswas, C. Kundu, W.L. Ng, S.P. Samudrala, T. Jarvis, S. Giddey, S. Bhattacharya, CO_2 valorisation to methane on highly stable iron impregnated ceria-zirconia based 3D-printed catalyst, J. CO_2 Util. 72 (2023), 102501, https://doi.org/10.1016/J.JCOU.2023.102501.

[23] A.I. Tsiotsias, N.D. Charisiou, I.V. Yentekakis, M.A. Goula, Bimetallic ni-based catalysts for co2 methanation: a review, Nanomaterials 11 (2021), https://doi.org/10.3390/nano11010028.

[24] W. Gac, W. Zawadzki, M. Rotko, M. Greluk, G. Słowik, G. Kolb, Effects of support composition on the performance of nickel catalysts in CO_2 methanation reaction, Catal. Today 357 (2020), https://doi.org/10.1016/j.cattod.2019.07.026.

[25] C. Lv, L. Xu, M. Chen, Y. Cui, X. Wen, Y. Li, C.E. Wu, B. Yang, Z. Miao, X. Hu, Q. Shou, Recent progresses in constructing the highly efficient Ni based catalysts

with advanced low-temperature activity toward CO_2 methanation, Front Chem. 8 (2020), https://doi.org/10.3389/fchem.2020.00269.
[26] Z. Wang, L. Wang, Y. Cui, Y. Xing, W. Su, Research on nickel-based catalysts for carbon dioxide methanation combined with literature measurement, J. CO_2 Util. 63 (2022), 102117, https://doi.org/10.1016/J.JCOU.2022.102117.
[27] L. Li, W. Zeng, M. Song, X. Wu, G. Li, C. Hu, Research progress and reaction mechanism of CO_2 methanation over Ni-based catalysts at low temperature: a review, Catalysts 12 (2022), https://doi.org/10.3390/catal12020244.
[28] J.Y. Do, N.K. Park, M.W. Seo, D. Lee, H.J. Ryu, M. Kang, Effective thermocatalytic carbon dioxide methanation on Ca-inserted NiTiO3 perovskite, Fuel 271 (2020), https://doi.org/10.1016/j.fuel.2020.117624.
[29] E.H. Cho, Y.K. Park, K.Y. Park, D. Song, K.Y. Koo, U. Jung, W.R. Yoon, C.H. Ko, Simultaneous impregnation of Ni and an additive via one-step melt-infiltration: Effect of alkaline-earth metal (Ca, Mg, Sr, and Ba) addition on Ni/γ-Al2O3 for CO_2 methanation, Chem. Eng. J. 428 (2022), https://doi.org/10.1016/j.cej.2021.131393.
[30] M.C. Bacariza, I. Graça, S.S. Bebiano, J.M. Lopes, C. Henriques, Magnesium as promoter of CO_2 methanation on Ni-based USY zeolites, Energy Fuels 31 (2017), https://doi.org/10.1021/acs.energyfuels.7b01553.
[31] L. Xu, H. Yang, M. Chen, F. Wang, D. Nie, L. Qi, X. Lian, H. Chen, M. Wu, CO_2 methanation over Ca doped ordered mesoporous Ni-Al composite oxide catalysts: the promoting effect of basic modifier, J. CO_2 Util. 21 (2017), https://doi.org/10.1016/j.jcou.2017.07.014.
[32] Q. Liu, B. Bian, J. Fan, J. Yang, Cobalt doped Ni based ordered mesoporous catalysts for CO_2 methanation with enhanced catalytic performance, Int J. Hydrog. Energy 43 (2018), https://doi.org/10.1016/j.ijhydene.2018.01.132.
[33] J. Tu, H. Wu, Q. Qian, S. Han, M. Chu, S. Jia, R. Feng, J. Zhai, M. He, B. Han, Low temperature methanation of CO 2 over an amorphous cobalt-based catalyst, Chem. Sci. 12 (2021) 3937–3943, https://doi.org/10.1039/D0SC06414A.
[34] N.D.M. Ridzuan, M.S. Shaharun, M.A. Anawar, I. Ud-Din, Ni-based catalyst for carbon dioxide methanation: a review on performance and progress, Catalysts 12 (2022), https://doi.org/10.3390/catal12050469.
[35] C. Liang, H. Tian, G. Gao, S. Zhang, Q. Liu, D. Dong, X. Hu, Methanation of CO_2 over alumina supported nickel or cobalt catalysts: Effects of the coordination between metal and support on formation of the reaction intermediates, Int J. Hydrog. Energy 45 (2020), https://doi.org/10.1016/j.ijhydene.2019.10.195.
[36] X. Yan, C. Yuan, J. Bao, S. Li, D. Qi, Q. Wang, B. Zhao, T. Hu, L. Fan, B. Fan, R. Li, F. Tao, Y.X. Pan, A Ni-based catalyst with enhanced Ni-support interaction for highly efficient CO methanation, Catal. Sci. Technol. 8 (2018), https://doi.org/10.1039/c8cy00605a.
[37] T.A. Le, J. Kim, J.K. Kang, E.D. Park, CO and CO_2 methanation over Ni/Al@Al2O3 core–shell catalyst, Catal. Today 356 (2020), https://doi.org/10.1016/j.cattod.2019.09.028.
[38] M. Younas, L. Loong Kong, M.J.K. Bashir, H. Nadeem, A. Shehzad, S. Sethupathi, Recent advancements, fundamental challenges, and opportunities in catalytic methanation of CO_2, Energy Fuels 30 (2016), https://doi.org/10.1021/acs.energyfuels.6b01723.
[39] M. Hervy, J. Maistrello, L. Brito, M. Rizand, E. Basset, Y. Kara, M. Maheut, Power-to-gas: CO_2 methanation in a catalytic fluidized bed reactor at demonstration scale, experimental results and simulation, J. CO_2 Util. 50 (2021), https://doi.org/10.1016/j.jcou.2021.101610.
[40] A. Catarina Faria, C.V. Miguel, A.E. Rodrigues, L.M. Madeira, Modeling and Simulation of a Steam-Selective Membrane Reactor for Enhanced CO2Methanation, Ind. Eng. Chem. Res 59 (2020), https://doi.org/10.1021/acs.iecr.0c02860.
[41] F.M. Baena-Moreno, M. González-Castaño, J.C. Navarro De Miguel, K.U.M. Miah, R. Ossenbrink, J.A. Odriozola, H. Arellano-García, Stepping toward Efficient Microreactors for CO2Methanation: 3D-Printed Gyroid Geometry, ACS Sustain Chem. Eng. 9 (2021), https://doi.org/10.1021/acssuschemeng.1c01980.
[42] H. Puliyalil, D. Lašič Jurković, V.D.B.C. Dasireddy, B. Likozar, A review of plasma-assisted catalytic conversion of gaseous carbon dioxide and methane into value-added platform chemicals and fuels, RSC Adv. 8 (2018), https://doi.org/10.1039/c8ra03146k.
[43] E. Jwa, S.B. Lee, H.W. Lee, Y.S. Mok, Plasma-assisted catalytic methanation of CO and CO_2 over Ni-zeolite catalysts, Fuel Process. Technol. (2013), https://doi.org/10.1016/j.fuproc.2012.03.008.
[44] M.A. Paviotti, L.A. Salazar Hoyos, V. Busilacchio, B.M. Faroldi, L.M. Cornaglia, Ni mesostructured catalysts obtained from rice husk ashes by microwave-assisted synthesis for CO2methanation, J. CO_2 Util. 42 (2020), https://doi.org/10.1016/j.jcou.2020.101328.
[45] F. Song, Q. Zhong, Y. Yu, M. Shi, Y. Wu, J. Hu, Y. Song, Obtaining well-dispersed Ni/Al2O3 catalyst for CO_2 methanation with a microwave-assisted method, Int J. Hydrog. Energy 42 (2017), https://doi.org/10.1016/j.ijhydene.2016.10.141.
[46] Y. Shen, Y. Dong, X. Han, J. Wu, K. Xue, M. Jin, G. Xie, X. Xu, Prediction model for methanation reaction conditions based on a state transition simulated annealing algorithm optimized extreme learning machine, Int J. Hydrog. Energy 48 (2023), https://doi.org/10.1016/j.ijhydene.2022.10.031.
[47] B. Yılmaz, B. Oral, R. Yıldırım, Machine learning analysis of catalytic CO_2 methanation, Int J. Hydrog. Energy 48 (2023), https://doi.org/10.1016/j.ijhydene.2022.12.197.
[48] J. Ren, Y.L. Liu, X.Y. Zhao, J.P. Cao, Methanation of syngas from biomass gasification: an overview, Int J. Hydrog. Energy 45 (2020), https://doi.org/10.1016/j.ijhydene.2019.12.023.
[49] A.S. Calbry-Muzyka, T.J. Schildhauer, Direct methanation of biogas—technical challenges and recent progress, Front Energy Res 8 (2020), https://doi.org/10.3389/fenrg.2020.570887.
[50] J. Witte, A. Calbry-Muzyka, T. Wieseler, P. Hottinger, S.M.A. Biollaz, T. J. Schildhauer, Demonstrating direct methanation of real biogas in a fluidised bed reactor, Appl. Energy 240 (2019), https://doi.org/10.1016/j.apenergy.2019.01.230.
[51] S. Carrasco-Ruiz, Q. Zhang, J. Gándara-Loe, L. Pastor-Pérez, J.A. Odriozola, T. R. Reina, L.F. Bobadilla, H2-rich syngas production from biogas reforming: overcoming coking and sintering using bimetallic Ni-based catalysts, Int J. Hydrog. Energy (2023), https://doi.org/10.1016/J.IJHYDENE.2023.03.301.
[52] J. González-Arias, M.E. Sánchez, E.J. Martínez, C. Covalski, A. Alonso-Simón, R. González, J. Cara-Jiménez, Hydrothermal carbonization of olive tree pruning as a sustainable way for improving biomass energy potential: effect of reaction parameters on fuel properties, Processes 8 (2020) 1201, https://doi.org/10.3390/PR8101201.
[53] J. Tan, J. Wang, Z. Zhang, Z. Ma, L. Wang, Y. Liu, Highly dispersed and stable Ni nanoparticles confined by MgO on ZrO2 for CO_2 methanation, Appl. Surf. Sci. 481 (2019) 1538–1548, https://doi.org/10.1016/J.APSUSC.2019.03.217.
[54] D. Han, Y. Kim, H. Byun, W. Cho, Y. Baek, Co2 methanation of biogas over 20 wt% ni-mg-al catalyst: on the effect of n2, ch4, and o2 on co2 conversion rate, Catalysts 10 (2020), https://doi.org/10.3390/catal10101201.
[55] Z. Liu, X. Ding, R. Zhu, Y. Li, Y. Wang, W. Sun, D. Wang, L. Wu, L. Zheng, Investigation on the effect of highly active Ni/ZrO2 catalysts modified by MgO-Nd2O3 promoters in CO_2 methanation at low temperature condition, ChemistrySelect 7 (2022), https://doi.org/10.1002/slct.202103774.
[56] J. Li, L. Zhou, Q. Zhu, H. Li, Enhanced methanation over aerogel NiCo/Al2O3 catalyst in a magnetic fluidized bed, Ind. Eng. Chem. Res 52 (2013), https://doi.org/10.1021/ie3030104.
[57] F. Rahbar Shamskar, M. Rezaei, F. Meshkani, The influence of Ni loading on the activity and coke formation of ultrasound-assisted co-precipitated Ni–Al2O3 nanocatalyst in dry reforming of methane, Int J. Hydrog. Energy 42 (2017), https://doi.org/10.1016/j.ijhydene.2016.11.067.
[58] X. He, W. Zhu, X. Wang, F. Wang, H. Liu, Z. Lei, Synthesis and color properties of the CoAl2O4/Al2O3 hybrid blue pigments with low cobalt contents, J. Mater. Sci. 55 (2020), https://doi.org/10.1007/s10853-020-04967-y.
[59] Z. Wei, H. Qiao, H. Yang, L. Zhu, X. Yan, Preparation and characterization of NiO nanoparticles by anodic arc plasma method, J. Nanomater 2009 (2009), https://doi.org/10.1155/2009/795928.
[60] G. Jayakumar, A.A. Irudayaraj, A.D. Raj, Particle size effect on the properties of cerium oxide (CeO2) manoparticles synthesized by hydrothermal method, Mech., Mater. Sci. Eng. J. 9 (2017).
[61] J.J. Villora-Picó, I. Campello-Gómez, J.C. Serrano-Ruiz, M.M. Pastor-Blas, A. Sepúlveda-Escribano, E.V. Ramos-Fernández, Hydrogenation of 4-nitrochloro-benzene catalysed by cobalt nanoparticles supported on nitrogen-doped activated carbon, Catal. Sci. Technol. 11 (2021), https://doi.org/10.1039/d1cy00140j.
[62] S. Andonova, C.N. de Ávila, K. Arishtirova, J.M.C. Bueno, S. Damyanova, Structure and redox properties of Co promoted Ni/Al2O3 catalysts for oxidative steam reforming of ethanol, Appl. Catal. B 105 (2011), https://doi.org/10.1016/j.apcatb.2011.04.029.
[63] V.O.O. Gonçalves, W.H.S.M. Talon, V. Kartnaller, F. Venancio, J. Cajaiba, T. Cabioc'h, J.M. Clacens, F. Richard, Hydrodeoxygenation of m-cresol as a depolymerized lignin probe molecule: synergistic effect of NiCo supported alloys, Catal. Today 377 (2021), https://doi.org/10.1016/j.cattod.2020.10.042.
[64] D.S. José-Alonso, M.J. Illán-Gómez, M.C. Román-Martínez, Low metal content Co and Ni alumina supported catalysts for the CO 2 reforming of methane, Int J. Hydrog. Energy 38 (2013), https://doi.org/10.1016/j.ijhydene.2012.11.080.
[65] J. Gandara-Loe, Q. Zhang, J.J. Villora-Picó, A. Sepúlveda-Escribano, L. Pastor-Pérez, T. Ramirez Reina, Design of full-temperature-range RWGS catalysts: impact of alkali promoters on Ni/CeO2, Energy Fuels 36 (2022), https://doi.org/10.1021/acs.energyfuels.2c00784.
[66] E.C. Faria, R.C.R. Neto, R.C. Colman, F.B. Noronha, Hydrogen production through CO_2 reforming of methane over Ni/CeZrO2/Al2O3 catalysts, : Catal. Today (2014), https://doi.org/10.1016/j.cattod.2013.10.058.
[67] A.L.A. Marinho, F.S. Toniolo, F.B. Noronha, F. Epron, D. Duprez, N. Bion, Highly active and stable Ni dispersed on mesoporous CeO2-Al2O3 catalysts for production of syngas by dry reforming of methane, Appl. Catal. B 281 (2021), https://doi.org/10.1016/j.apcatb.2020.119459.
[68] L. Yang, L. Pastor-Pérez, S. Gu, A. Sepúlveda-Escribano, T.R. Reina, Highly efficient Ni/CeO2-Al2O3 catalysts for CO_2 upgrading via reverse water-gas shift: effect of selected transition metal promoters, Appl. Catal. B 232 (2018), https://doi.org/10.1016/j.apcatb.2018.03.091.
[69] L.P. Matte, A.S. Kilian, L. Luza, M.C.M. Alves, J. Morais, D.L. Baptista, J. Dupont, F. Bernardi, Influence of the CeO2 support on the reduction properties of Cu/CeO2 and Ni/CeO2 nanoparticles, J. Phys. Chem. C. 119 (2015), https://doi.org/10.1021/acs.jpcc.5b07654.
[70] X. Li, X. Liu, J. Hao, L. Li, Y. Gao, Y. Gu, Z. Cao, J. Liu, Strong metal–support interactions of Ni-CeO $_2$ effectively improve the performance of a molten hydroxide direct carbon fuel cell, ACS Omega 7 (2022) 24646–24655, https://doi.org/10.1021/acsomega.2c02479.
[71] I.U. Din, M.A. Alotaibi, A.I. Alharthi, A. Naeem, G. Centi, Synthesis, characterization and activity of CeO2 supported Cu-Mg bimetallic catalysts for CO_2 to methanol, Chem. Eng. Res. Des. 192 (2023), https://doi.org/10.1016/j.cherd.2023.02.030.
[72] B. Alrafei, I. Polaert, A. Ledoux, F. Azzolina-Jury, Remarkably stable and efficient Ni and Ni-Co catalysts for CO_2 methanation, Catal. Today 346 (2020), https://doi.org/10.1016/j.cattod.2019.03.026.

[73] M.M. Jaffar, M.A. Nahil, P.T. Williams, Parametric study of CO_2 methanation for synthetic natural gas production, Energy Technol. 7 (2019), https://doi.org/10.1002/ente.201900795.
[74] P. Summa, K. Świrk, Y. Wang, B. Samojeden, M. Rønning, C. Hu, M. Motak, P. Da Costa, Effect of cobalt promotion on hydrotalcite-derived nickel catalyst for CO_2 methanation, Appl. Mater. Today 25 (2021), https://doi.org/10.1016/j.apmt.2021.101211.
[75] P. Shafiee, S.M. Alavi, M. Rezaei, Solid-state synthesis method for the preparation of cobalt doped Ni–Al2O3 mesoporous catalysts for CO_2 methanation, Int J. Hydrog. Energy 46 (2021), https://doi.org/10.1016/j.ijhydene.2020.10.221.
[76] U.P.M. Ashik, W.M.A. Wan Daud, H.F. Abbas, Production of greenhouse gas free hydrogen by thermocatalytic decomposition of methane - a review, Renew. Sustain. Energy Rev. 44 (2015), https://doi.org/10.1016/j.rser.2014.12.025.
[77] L. Alves, V. Pereira, T. Lagarteira, A. Mendes, Catalytic methane decomposition to boost the energy transition: scientific and technological advancements, Renew. Sustain. Energy Rev. 137 (2021), https://doi.org/10.1016/j.rser.2020.110465.
[78] M. Msheik, S. Rodat, S. Abanades, Methane cracking for hydrogen production: a review of catalytic and molten media pyrolysis, Energ. (Basel) 14 (2021), https://doi.org/10.3390/en14113107.
[79] J. González-Arias, G. Torres-Sempere, F. Arroyo-Torralvo, T.R. Reina, J. A. Odriozola, Optimizing biogas methanation over nickel supported on ceria-alumina catalyst: towards CO_2-rich biomass utilization for a negative emissions society, Environ. Res 242 (2024), 117735, https://doi.org/10.1016/j.envres.2023.117735.
[80] Q. Zhang, M. Bown, L. Pastor-Pérez, M.S. Duyar, T.R. Reina, CO2Conversion via reverse water gas shift reaction using fully selective Mo-P multicomponent catalysts, Ind. Eng. Chem. Res 61 (2022), https://doi.org/10.1021/acs.iecr.2c00305.
[81] Z. Tian, H. Yang, Q. Liu, CO methanation on mesoporous Ni–VOx/FDU-12 catalyst: effects of the VOx promoter on low-temperature activity, Energy Technol. 8 (2020), 1901270, https://doi.org/10.1002/ENTE.201901270.
[82] J. Friedland, T. Turek, R. Güttel, Study on the tolerance of low-temperature CO methanation with single pulse experiments, Chem. Eng. J. 443 (2022), https://doi.org/10.1016/j.cej.2022.136262.
[83] R. Daroughegi, F. Meshkani, M. Rezaei, Enhanced low-temperature activity of CO_2 methanation over ceria-promoted Ni-Al2O3 nanocatalyst, Chem. Eng. Sci. 230 (2021), https://doi.org/10.1016/j.ces.2020.116194.
[84] G. Varvoutis, M. Lykaki, S. Stefa, V. Binas, G.E. Marnellos, M. Konsolakis, Deciphering the role of Ni particle size and nickel-ceria interfacial perimeter in the low-temperature CO_2 methanation reaction over remarkably active Ni/CeO2 nanorods, Appl. Catal. B 297 (2021), https://doi.org/10.1016/j.apcatb.2021.120401.
[85] Y. Xie, J. Wen, Z. Li, J. Chen, Q. Zhang, P. Ning, Y. Chen, J. Hao, Progress in reaction mechanisms and catalyst development of ceria-based catalysts for low-temperature CO_2 methanation, Green. Chem. 25 (2022), https://doi.org/10.1039/d2gc03512j.
[86] I. Iglesias, A. Quindimil, F. Mariño, U. De-La-Torre, J.R. González-Velasco, Zr promotion effect in CO_2 methanation over ceria supported nickel catalysts, Int J. Hydrog. Energy 44 (2019) 1710–1719, https://doi.org/10.1016/J.IJHYDENE.2018.11.059.
[87] E. Le Saché, J.L. Santos, T.J. Smith, M.A. Centeno, H. Arellano-Garcia, J. A. Odriozola, T.R. Reina, Multicomponent Ni-CeO2 nanocatalysts for syngas production from CO_2/CH4 mixtures, J. CO_2 Util. 25 (2018), https://doi.org/10.1016/j.jcou.2018.03.012.
[88] H. Liu, X. Zou, X. Wang, X. Lu, W. Ding, Effect of CeO2 addition on Ni/Al2O3 catalysts for methanation of carbon dioxide with hydrogen, J. Nat. Gas. Chem. 21 (2012), https://doi.org/10.1016/S1003-9953(11)60422-2.